AIAA SciTech Forum
7-11 January 2019, San Diego, California
AIAA Scitech 2019 Forum

10.2514/6.2019-0438

A multifidelity method for locating aeroelastic flutter boundaries

Alexandre N. Marques*, Remi R. Lam†, Anirban Chaudhuri‡, and Max M. J. Opgenoord§
Massachusetts Institute of Technology, Cambridge, MA, 02139

Karen E. Willcox¶
University of Texas at Austin, Austin, TX 78712

Aeroelastic flutter is a dangerous dynamic instability that can affect aerospace vehicles in certain flight conditions. Producing an accurate estimate of the aeroelastic flutter boundary is a challenge because high-fidelity aeroelastic models (e.g., based on fluid-structure interaction) are expensive to evaluate, and aeroelastic flutter analysis requires a large number of model evaluations. Many relatively inexpensive approximate aeroelastic models (low-fidelity models) exist, and are routinely applied to reduce the cost of estimating aeroelastic flutter. We introduce a multifidelity method that can produce accurate estimates of the aeroelastic flutter boundary by combining information from low- and high-fidelity models This method constructs a mulifidelity statistical surrogate to fit data from all available models, learning the correlations between them. The statistical surrogate is used to measure the uncertainty in the aeroelastic flutter boundary predicted with a given set of model evaluations. The method then automatically selects new model evaluations using an active learning approach such that the uncertainty in the estimate of aeroelastic flutter boundary is reduced the most, by unit cost, at every iteration. We demonstrate the effectiveness of the multifidelity method by locating the aeroelastic flutter boundary of a typical section model.

Nomenclature

$\mathcal{A}$	=	convective and diffusive phenomena that govern the airflow dynamics
b	=	semi-chord length
c_ℓ	=	lift coefficient
c_m	=	momentum coefficient, with respect to the elastic axis
d_j	=	damping of aeroelastic mode j
f	=	Gaussian process surrogate model
F_a	=	aerodynamic forces
F_el	=	elastic forces
K	=	stiffness matrix
M	=	mass matrix
m_a	=	mass of airfoil
m	=	mean function in Gaussian process surrogate model
M_∞	=	Mach number at freestream
p	=	cost of evaluating aeroelastic model
q_∞	=	dynamic pressure at freestream
r_θ	=	radius of gyration per span about the elastic axis
V_∞	=	speed at freestream
V_μ	=	speed index, $V_\infty/\sqrt{\mu}b\omega_\theta$
$\boldsymbol{x}$	=	vector of parameters that affect aeroelastic stability

*Postdoctoral Associate, Department of Aeronautics and Astronautics, AIAA Member.
†Postdoctoral Associate, Department of Aeronautics and Astronautics, AIAA Member.
‡Postdoctoral Associate, Department of Aeronautics and Astronautics, AIAA Member.
§Postdoctoral Associate, Department of Aeronautics and Astronautics, AIAA Member.
¶Professor, Institute for Computational Engineering and Sciences, AIAA Associate Fellow.

x_{cg} = position of center of gravity in semi-chords, measured from mid-chord
x_{ea} = position of elastic axis in semi-chords, measured from mid-chord
γ = aeroelastic damping coefficient
$\boldsymbol{\eta}$ = degrees-of-freedom of structure
$\boldsymbol{\eta}_a$ = degrees-of-freedom of airflow
μ = mass ratio, $\mu = m_a/\pi\rho_\infty b^2$
Σ = covariance kernel in Gaussian process surrogate model
ω_j = angular frequency of aeroelastic mode j
ω_θ = uncoupled natural angular frequency of pitch mode in vacuum, in rad/s
ω_h = uncoupled natural angular frequency of heave mode in vacuum, in rad/s
ρ_∞ = density at freestream
θ = pitch angle, in radians
ξ = heave displacement, in semi-chords

I. Introduction

Aeroelastic flutter is a dynamic instability that can affect aerospace vehicles in certain flight conditions, and results in dangerous structural oscillations. The aeroelastic flutter boundary is the set of parameters (Mach number, speed, etc.) that separates stable and unstable conditions. One relatively simple approach to estimate the aeroelastic flutter boundary is the method of bisection, illustrated in the left frame of Fig. 1. However, producing an accurate estimate based on bisection is a challenge because it requires many evaluations of the aeroelastic model, and accurate (high-fidelity) aeroelastic models are expensive to evaluate. We present a multifidelity method that produces accurate estimates of aeroelastic flutter boundaries at relatively low cost by leveraging information from inexpensive and approximate (low-fidelity) aeroelastic models. As illustrated in the right frame of Fig. 1, the multifidelity method uses only a small number of evaluations of the high-fidelity aeroelastic model to guarantee the accuracy of the estimated aeroelastic flutter boundary.

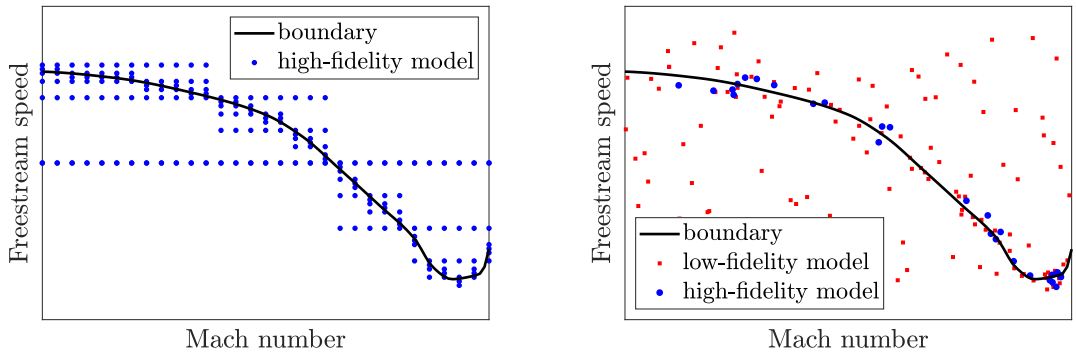

Fig. 1 Left: illustration of bisection method to find the aeroelastic flutter boundary. This method requires many evaluations of the high-fidelity aeroelastic model to find the entire flutter boundary. Right: illustration of the multifidelity method presented here. The multifidelity method uses evaluations of relatively cheap low-fidelity aeroelastic models to reduce the overall cost of aeroelastic flutter analysis.

In principle, fluid-structure interaction (FSI) simulations are the most accurate representations of aeroelastic phenomena. However, despite advances [1–11], FSI remains too expensive for routine aeroelastic flutter analysis in engineering design. For this reason, low-fidelity aeroelastic models have been developed and are routinely used. One common type of low-fidelity aeroelastic model is based on the linearized potential flow approximation [12–16]. These models are considerably cheaper than FSI, and perform well in the low subsonic regime. On the other hand, there are important non-linear phenomena that are not represented adequately by linearized potential flow models. One example is the *transonic dip*, an abrupt decrease in flutter speed that may occur in the transonic regime, as illustrated in Fig. 2. Other types of aeroelastic model are based on measuring the aerodynamic response to small perturbations of the structure

using high-fidelity simulations, and fitting the results with linearized models [17–25]. In addition, reduced order modeling [26] is often used to identify a lower-dimensional (and therefore cheaper) model of the aeroelastic response, using methods such as proper orthogonal decomposition [27–29], harmonic balance [30], and Volterra series [31].

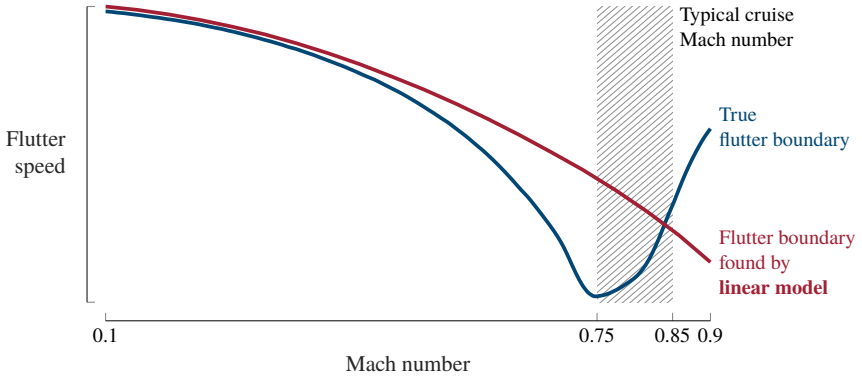

Fig. 2 Transonic dip: flutter speed can decrease abruptly in the transonic region. This phenomenon is not predicted by linearized aerodynamic models. Figure reproduced from Ref. [32] with permission.

The multifidelity method we introduce here is based on principles of active learning, where model evaluations are selected iteratively based on how much they are estimated to improve predictions [33]. In this context, the problem of locating the aeroelastic flutter boundary can have two interpretations, leading to different methodologies.

The first interpretation is as a classification problem: aeroelastic configurations can be stable or unstable, and the aeroelastic flutter boundary separates the two categories. Support vector machine (SVM) [34–37] is a technique widely adopted to construct classifiers. Missoum et al. [38] applied an adaptive SVM algorithm to reduce the cost of reliability-based design optimization of aeroelastic problems, whereas Dribusch et al. [39] applied a multifidelity adaptive SVM to estimate an aeroelastic flutter boundary.

The second interpretation is as a contour location problem: the aeroelastic flutter boundary is the zero contour of the aeroelastic damping coefficient. Active learning algorithms based on Gaussian process surrogates [40–45] are commonly used to locate contours of expensive-to-evaluate functions. The present method lies in this category. This method is based on CLoVER [46], an active learning algorithm that combines information from multiple sources. An important distinction between the present method and the work of Dirbusch et al. [39] is that we do not require any hierarchy between the different aeroelastic models. In contrast, the multifidelity method of Dribusch et al. [39] assumes that a hierarchy between the fidelities of the models exists and is known.

The remainder of this paper is organized as follows. In Sect. II we present a formal definition of the aeroelastic flutter boundary. In Sect. III we discuss the details of the multifidelity method. We apply this method to locate the aeroelastic flutter boundary of a typical section problem, and the results are in Sect. IV. Finally, in Sect. V we discuss conclusions and opportunities for future work.

II. Aeroelastic flutter

The behavior of an aeroelastic system is governed by the dynamics of the structure under the influence of aerodynamic forces. Here we represent the state of the structure and airflow by discrete sets of degrees-of-freedom. The vector of generalized coordinates (translations/rotations, structural modes) $\boldsymbol{\eta} \in \mathbb{R}^N$ defines the state of the structure, while the vector of flow variables (velocity, gas properties) $\boldsymbol{\eta}_a \in \mathbb{R}^{N_a}$ defines the state of the airflow. The dynamics of a general aeroelastic system are governed by

$$M\ddot{\boldsymbol{\eta}} + F_{\text{el}}(\boldsymbol{\eta}) = F_{\text{a}}(\boldsymbol{\eta}_a, q_\infty), \tag{1a}$$

$$\dot{\boldsymbol{\eta}}_a = \mathcal{A}(M_\infty, \text{Re}, \boldsymbol{\eta}_a, \boldsymbol{\eta}), \tag{1b}$$

where M is the mass matrix, F_{el} denotes elastic forces, F_{a} denotes aerodynamic forces acting on the structure, and $\mathcal{A}$ represents convective and diffusive phenomena that govern the evolution of the airflow – e.g., (1b) can represent the Navier-Stokes equations. In addition, q_∞ is the dynamic pressure, M_∞ is the Mach number, and Re is the Reynolds number, all measured in freestream conditions.

Let $\{\boldsymbol{\eta}_0, \boldsymbol{\eta}_{a_0}\}$ denote a state of aeroelastic equilibrium, i.e.,

$$\begin{aligned} F_{\text{el}}(\boldsymbol{\eta}_0) &= F_{\text{a}}(\boldsymbol{\eta}_{a_0}, q_\infty), \\ \mathcal{A}(M_\infty, \text{Re}, \boldsymbol{\eta}_{a_0}, \boldsymbol{\eta}_0) &= 0. \end{aligned} \tag{2}$$

Aeroelastic flutter is characterized by the response of the aeroelastic system (1), initially at equilibrium, to an infinitesimal disturbance $\boldsymbol{\delta\eta}$. In the infinitesimal limit, the response of the structure can be approximated as linear with respect to the disturbance magnitude:

$$\boldsymbol{\eta}(t) = \boldsymbol{\eta}_0 + ||\boldsymbol{\delta\eta}|| \sum_{j=1}^{N} \bar{\boldsymbol{\eta}}_j e^{(d_j + i\omega_j)t},$$

where $\bar{\boldsymbol{\eta}}_j$ denotes the $j-$th mode of vibration of the aeroelastic system (out of a total of N modes), with damping d_j and angular frequency ω_j. Let J denote the vibration mode with largest damping, i.e., $d_J = \max_j d_j$. This mode determines the stability of the aeroelastic system: $d_J = 0$ indicates the onset of aeroelastic flutter, and the system is said to flutter if $d_J > 0$. Aeroelastic damping is also commonly described in terms of the damping coefficient: $\gamma = d_J/\omega_J$.

Let $\boldsymbol{x}$ denote the vector of parameters that affect the stability of the aeroelastic system (e.g., Mach number, speed, mass, stiffness, etc.). The *aeroelastic flutter boundary* is defined as the set of conditions

$$\mathcal{Z} = \{\boldsymbol{x} \mid \gamma(\boldsymbol{x}) = 0\}. \tag{3}$$

III. A multifidelity method for aeroelastic flutter analysis

The multifidelity method proposed here is based on CLoVER (**C**ontour **Lo**cation **V**ia **E**ntropy **R**eduction) [46], an active learning algorithm that combines information from multiple models to locate the zero contour of an expensive-to-evaluate function. In the case of aeroelastic flutter analysis, one wants to locate the flutter boundary, which corresponds to the zero contour of the aeroelastic damping coefficient $\gamma = \gamma(\boldsymbol{x})$. In general, high-fidelity evaluations of γ are expensive. The present method leverages information from low-fidelity aeroelastic models to estimate the flutter boundary accurately at a reasonable cost. In Sect. III.A we explain what constitutes an aeroelastic model, and establish the notation for the remainder of this section.

The multifidelity method has three main ingredients:

- A multifidelity statistical surrogate model that fits data from low- and high-fidelity aeroelastic models, encoding correlations between the different fidelities. We discuss the surrogate model in Sect. III.B.
- A measure of uncertainty about the location of the flutter boundary estimated by the statistical surrogate model, as detailed in Sect. III.C.
- A decision mechanism that selects which model and aeroelastic condition to evaluate next such that the uncertainty about the location of the flutter boundary is reduced the most, per unit computational cost. We discuss this mechanism in Sect. III.D.

Finally, in Sect. III.E we show how these ingredients are combined to form the multifidelity method.

A. Aeroelastic models and notation

In this paper, the term *aeroelastic model* is used to designate the combination of modeling assumptions, numerical discretizations, and numerical algorithms used to:

(i) describe the operators F_{el}, F_{a}, and $\mathcal{A}$,
(ii) solve the aeroelastic problem (1), and
(iii) estimate the aeroelastic damping coefficient, defined by (2).

We assume that we have access to N_m aeroelastic models, each of which provides an estimate of the damping coefficient γ. We denote the estimate from model ℓ as γ_ℓ, made with computational cost p_ℓ, $\ell \in \{0, \ldots, N_m - 1\}$.

Let $\ell = 0$ denote the aeroelastic model in which we have the highest confidence, i.e., the model that results in our most accurate (and likely most expensive) estimate of aeroelastic damping coefficient. We refer to aeroelastic model $\ell = 0$ as the *high-fidelity model*, and aim to estimate the aeroelastic flutter boundary defined by

$$\mathcal{Z}_0 = \{\boldsymbol{x} \mid \gamma_0(\boldsymbol{x}) = 0\}. \tag{4}$$

The aeroelastic models $\ell = 1, \ldots, N_m - 1$ are referred to as *low-fidelity models*.

B. Multifidelity surrogate model

We use the statistical surrogate model introduced by Poloczek et al. [47] in the context of multi-information source optimization. This model constructs a single Gaussian process (GP) surrogate that simultaneously approximates the low- and high-fidelity models, and thus exploits relationships between them.

Let f denote the surrogate model, with $f(\ell, \boldsymbol{x})$ being the GP that represents the belief about function $\gamma_\ell(\boldsymbol{x})$, $\ell = 0, \ldots, N_m - 1$. The construction of the surrogate follows from two modeling choices:

(i) a GP approximation to $\gamma_0(\boldsymbol{x})$ denoted by $f(0, \boldsymbol{x})$, i.e., $f(0, \boldsymbol{x}) \sim GP(m_0, \Sigma_0)$, and

(ii) independent GP approximations to the discrepancies $\delta_\ell(\boldsymbol{x}) = \gamma_\ell(\boldsymbol{x}) - \gamma_0(\boldsymbol{x})$, i.e., $\delta_\ell \sim GP(m_\ell, \Sigma_\ell)$ with $\mathrm{Cov}(\delta_\ell(\boldsymbol{x}), f(0, \boldsymbol{x}')) = 0$ and $\mathrm{Cov}(\delta_\ell(\boldsymbol{x}), \delta_{\ell'}(\boldsymbol{x}')) = \mathbb{1}_{\ell,\ell'}\Sigma_\ell(\boldsymbol{x}, \boldsymbol{x}')$, where $\mathbb{1}_{\ell,\ell'}$ denotes the Kronecker's delta.

In the definitions above, m_ℓ denotes the mean function and Σ_ℓ denotes the covariance kernel of the GP $f(\ell, \boldsymbol{x})$. As a consequence of these modeling choices, the surrogate model $f(\ell, \boldsymbol{x}) = f(0, \boldsymbol{x}) + \delta_\ell(\boldsymbol{x})$ is also a GP, $f \sim GP(m, \Sigma)$, with

$$\begin{aligned} m(\ell, \boldsymbol{x}) &= \mathbb{E}[f(\ell, \boldsymbol{x})] \\ &= \mathbb{E}[f(0, \boldsymbol{x})] + \mathbb{E}[\delta_\ell(\boldsymbol{x})] \\ &= m_0(\boldsymbol{x}) + m_\ell(\boldsymbol{x}), \end{aligned} \tag{5}$$

$$\begin{aligned} \Sigma\big((\ell, \boldsymbol{x}), (\ell', \boldsymbol{x}')\big) &= \mathrm{Cov}\big(f(\ell, \boldsymbol{x}), f(\ell', \boldsymbol{x}')\big) \\ &= \mathrm{Cov}\Big(\big(f(0, \boldsymbol{x}) + \delta_\ell(\boldsymbol{x})\big), \big(f(0, \boldsymbol{x}') + \delta_{\ell'}(\boldsymbol{x}')\big)\Big) \\ &= \mathrm{Cov}\big(f(0, \boldsymbol{x}), f(0, \boldsymbol{x}')\big) + \mathrm{Cov}\big(\delta_\ell(\boldsymbol{x}), \delta_{\ell'}(\boldsymbol{x}')\big) + \mathrm{Cov}\big(f(0, \boldsymbol{x}), \delta_{\ell'}(\boldsymbol{x}')\big) + \mathrm{Cov}\big(f(0, \boldsymbol{x}'), \delta_\ell(\boldsymbol{x})\big) \\ &= \Sigma_0(\boldsymbol{x}, \boldsymbol{x}') + \mathbb{1}_{\ell,\ell'}\Sigma_\ell(\boldsymbol{x}, \boldsymbol{x}'). \end{aligned} \tag{6}$$

Note that the multifidelity surrogate model $f(\ell, \boldsymbol{x})$ is a standard GP with a particular form of mean function, Eq. (5), and covariance kernel, Eq. (6). Therefore, assimilating data follows from standard tools of Gaussian process regression [48]. One important consequence of this surrogate construction is that low-fidelity data affect the surrogate representation of the high-fidelity model. Figure 3 illustrates this effect.

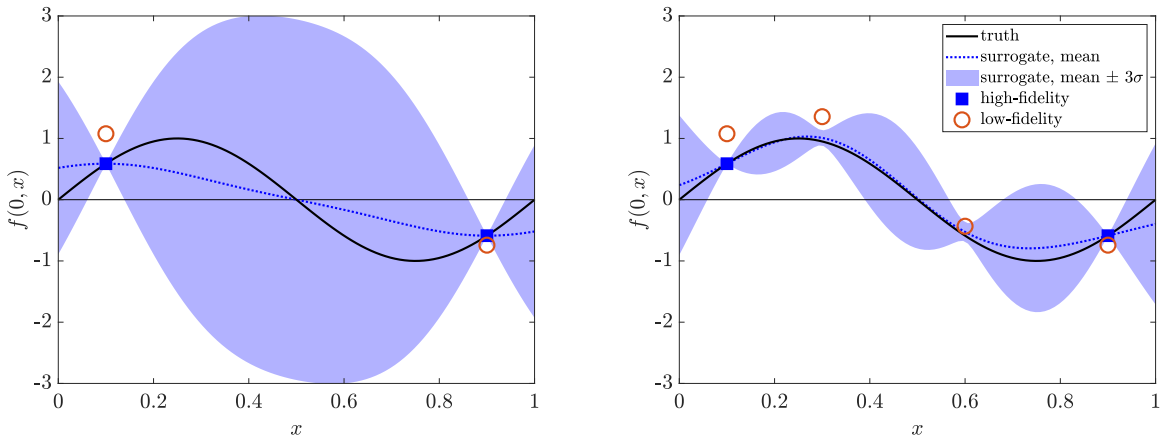

Fig. 3 Low-fidelity data improves prediction of high-fidelity function. Left: two observations of low- and high-fidelity models. Multifidelity surrogate fits high-fidelity data and learns correlation between different models. Right: two additional observations of the low-fidelity model result in significant improvement of surrogate representation of high-fidelity model.

In practice, m_ℓ and Σ_ℓ are selected from one of the standard parameterized classes of mean functions and covariance kernels [48]. The parameters of these functions and kernels (known as hyperparameters) are selected using maximum likelihood estimate (MLE) [48]. To mitigate difficulties associated with estimating hyperparameters with small amounts of data, the multifidelity method updates its estimate of hyperparameters throughout the evolution of the algorithm.

Namely, whenever the high-fidelity model is evaluated, all low-fidelity models are also evaluated, and the discrepancies between the models are used to recompute the hyperparameters.

C. Flutter boundary uncertainty

We measure the uncertainty about the location of the flutter boundary by applying the concept of *contour entropy* [46] to the surrogate model discussed above. Contour entropy measures the uncertainty of the zero contour estimated by a statistical surrogate model by defining a discrete random variable associated with point-wise predictions and integrating the associated entropy.*

For any given condition $\boldsymbol{x}$, the aeroelastic system is stable ($\gamma_0(\boldsymbol{x}) < 0$), unstable ($\gamma_0(\boldsymbol{x}) < 0$), or in neutral equilibrium ($\gamma_0(\boldsymbol{x}) = 0$). The surrogate model $f(0,\boldsymbol{x})$, conditioned on all available evaluations, is a normal random variable with known mean $m(0,\boldsymbol{x})$ and variance $\sigma^2(0,\boldsymbol{x})$, which allows us to estimate the aeroelastic stability and quantify the uncertainty in this estimate. In order to quantify the neutral equilibrium state, we relax the definition of the flutter boundary to $|\gamma_0(\boldsymbol{x})| < \epsilon(\boldsymbol{x})$, where $\epsilon(\boldsymbol{x})$ is a small positive number. Then, an observation y of $f(0,\boldsymbol{x})$ can be classified as one of the following three events:

- $y < -\epsilon(\boldsymbol{x})$ (stable, denoted as event S),
- $|y| < \epsilon(\boldsymbol{x})$ (neutral equilibrium, denoted as event E), or
- $y > \epsilon(\boldsymbol{x})$ (unstable, denoted as event U).

These three events define a discrete random variable, $W_{\boldsymbol{x}}$, with probability mass

$$P(S) = \Phi\left(\frac{-m(0,\boldsymbol{x}) - \epsilon(\boldsymbol{x})}{\sigma(0,\boldsymbol{x})}\right),$$

$$P(E) = \Phi\left(\frac{-m(0,\boldsymbol{x}) + \epsilon(\boldsymbol{x})}{\sigma(0,\boldsymbol{x})}\right) - \Phi\left(\frac{-m(0,\boldsymbol{x}) - \epsilon(\boldsymbol{x})}{\sigma(0,\boldsymbol{x})}\right),$$

$$P(U) = \Phi\left(\frac{m(0,\boldsymbol{x}) - \epsilon(\boldsymbol{x})}{\sigma(0,\boldsymbol{x})}\right),$$

where Φ is the unit normal cumulative distribution function. Figure 4 illustrates events S, E, and U, and the probability mass associated with each of them. It was shown in Ref. [46] that $\epsilon(\boldsymbol{x}) = 2\sigma(0,\boldsymbol{x})$ offers a good compromise between exploration and exploitation.

The entropy of $W_{\boldsymbol{x}}$ measures the uncertainty in the stabiltity of the aerolastic system at condition $\boldsymbol{x}$, and is given by

$$H(W_{\boldsymbol{x}}; f) = -P(S)\ln P(S) - P(E)\ln P(E) - P(U)\ln P(U). \tag{7}$$

Let $\mathcal{D}$ denote the range of airflow parameters considered for aeroelastic flutter analysis (e.g., the flight envelope of an aerospace vehicle). To characterize the uncertainty of the flutter boundary predicted by the surrogate model we measure the *contour entropy*, defined as

$$\mathscr{H}(f) = \frac{1}{V(\mathcal{D})}\int_{\mathcal{D}} H(W_{\boldsymbol{x}}; f)\, d\boldsymbol{x}, \tag{8}$$

where $V(\mathcal{D})$ denotes the volume of the parameter domain $\mathcal{D}$. The bottom left pane of Fig. 4 depicts the definition of contour entropy.

D. Selecting new evaluations

At each new iteration the multifidelity method selects which aeroelastic model ℓ and aeroelastic condition $\boldsymbol{x}$ to evaluate such that the uncertainty in the estimate of flutter boundary is reduced the most, per unit computational cost.

Consider the algorithm after n samples evaluated at $X_n = \{(\ell^i, \boldsymbol{x}^i)\}_{i=1}^n$, which result in observations $Y_n = \{\gamma_{\ell^i}(x^i)\}_{i=1}^n$. We denote the posterior GP of f, conditioned on $\{X_n, Y_n\}$, as f^n, with mean m^n and covariance matrix Σ^n. Then, the multifidelity method selects ℓ and $\boldsymbol{x}$ for a new evaluation by solving the following optimization problem.

$$\underset{\ell\in\{0,\ldots,M\},\,\boldsymbol{x}\in\mathcal{D}}{\text{maximize}} \quad u(\ell,\boldsymbol{x}; f^n), \tag{9}$$

*In information theory, entropy is a measure of the uncertainty in the outcome of a random process [49].

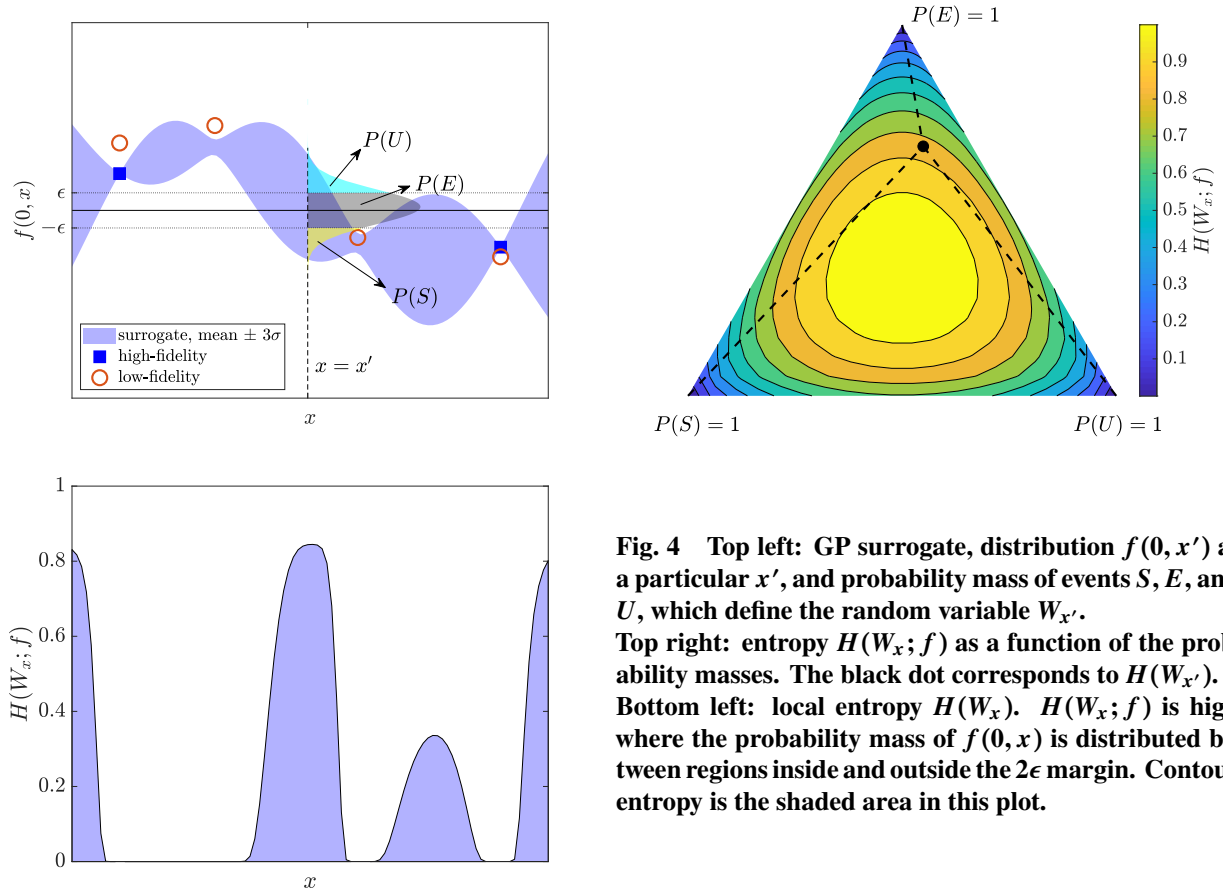

Fig. 4 Top left: GP surrogate, distribution $f(0, x')$ at a particular x', and probability mass of events S, E, and U, which define the random variable $W_{x'}$. Top right: entropy $H(W_x; f)$ as a function of the probability masses. The black dot corresponds to $H(W_{x'})$. Bottom left: local entropy $H(W_x)$. $H(W_x; f)$ is high where the probability mass of $f(0, x)$ is distributed between regions inside and outside the 2ϵ margin. Contour entropy is the shaded area in this plot.

where

$$u(\ell, \boldsymbol{x}; f^n) = \frac{\mathbb{E}_y[\mathscr{H}(f^n) - \mathscr{H}(f^{n+1}) \mid \ell^{n+1} = \ell,\, \boldsymbol{x}^{n+1} = \boldsymbol{x}]}{p_\ell(\boldsymbol{x})}, \tag{10}$$

and the expectation is taken over the distribution of possible observations, $y^{n+1} \sim \mathcal{N}\big(m^n(\ell, \boldsymbol{x}), \Sigma^n((\ell, \boldsymbol{x}), (\ell, \boldsymbol{x}))\big)$. There is no exact closed form expression for computing the expectation in (10), but Ref. [46] shows an approximate expression that can be computed without numerical integration. With this approximation, the utility function (10) can be evaluated as

$$u(\ell, \boldsymbol{x}; f^n) \approx \frac{1}{V(\mathcal{D})} \int_{\mathcal{D}} H(W_{x'}; f^n) - \frac{r_\sigma(\boldsymbol{x}'; \ell, \boldsymbol{x})}{e} \sum_{i=0}^{1} \sum_{j=0}^{1} \exp\left(-\frac{1}{2} \left(\frac{m^n(0, \boldsymbol{x}') + (-1)^i \epsilon}{\hat{\sigma}(\boldsymbol{x}'; \ell, \boldsymbol{x})} + (-1)^j \beta r_\sigma(\boldsymbol{x}'; \ell, \boldsymbol{x}) \right)^2 \right) d\boldsymbol{x}', \tag{11}$$

where $\beta = \Phi^{-1}(e^{-1})$ and

$$\hat{\sigma}^2(\boldsymbol{x}'; \ell, \boldsymbol{x}) = \Sigma^{n+1}((0, \boldsymbol{x}'), (0, \boldsymbol{x}')) + \frac{\big(\Sigma^n((0, \boldsymbol{x}'), (\ell, \boldsymbol{x}))\big)^2}{\Sigma^n((\ell, \boldsymbol{x}), (\ell, \boldsymbol{x}))},$$

$$r_\sigma^2(\boldsymbol{x}'; \ell, \boldsymbol{x}) = \frac{\Sigma^{n+1}((0, \boldsymbol{x}'), (0, \boldsymbol{x}'))}{\hat{\sigma}^2(\boldsymbol{x}'; \ell, \boldsymbol{x})}.$$

The integral over $\mathcal{D}$ is computed numerically using the importance sampling approach proposed in Ref. [44].

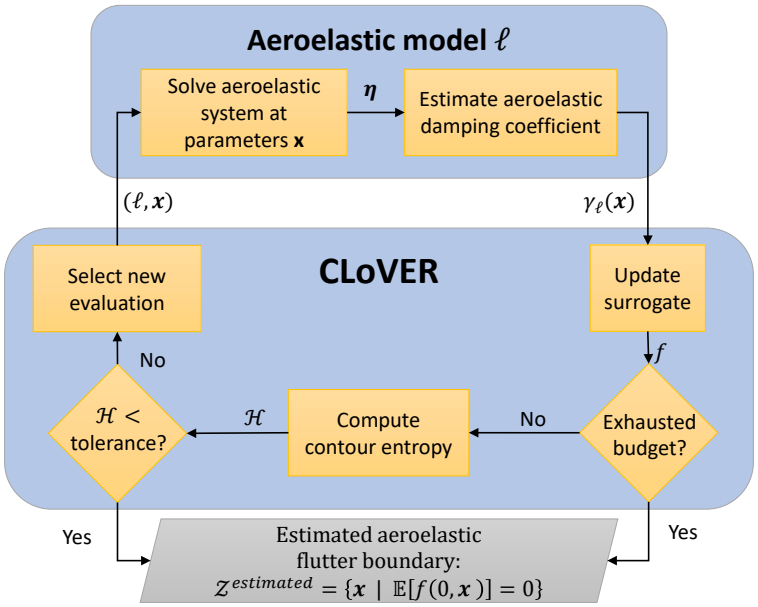

Fig. 5 Schematic representation of the multifidelity method for aeroelastic flutter analysis. The algorithm CLoVER combines data from multiple aeroelastic models to train a statistical surrogate model (denoted by f) of the aeroelastic damping coefficient. The surrogate is then used as a generative model to select which aeroelastic model and airflow condition to evaluate next.

E. Assembling the full method

The multifidelity method for aeorelastic flutter analysis can be summarized as follows (see Fig. 5):[†]

1) Compute an initial set of samples by evaluating all $N_m + 1$ aeroelastic models at the same values of $\boldsymbol{x}$. Use samples to compute hyperparameters and the posterior of f.
2) Until budget is exhausted, do:
    1) Determine which aeroelastic model and condition to sample next by solving the optimization problem (9).
    2) Evaluate the next sample at location x^{n+1} using aeroelastic model ℓ^{n+1}.
    3) Update hyperparameters and posterior of f.
3) Return the zero contour of $\mathbb{E}[f(0, \boldsymbol{x})]$.

IV. Aeroelastic flutter analysis of Isogai case A

A. Problem description

In this example we apply the multifidelity method to locate the aeroelastic flutter boundary of the aeroelastic system "case A" introduced by Isogai [1, 25, 50]. This system is an instance of a typical section model, which represents the aeroelastic behavior of a rigid airfoil supported by linear translation and torsion springs (see Fig. 6) [12, 51]. This model is used to represent the behavior of sections of wings in simplified aeroelastic analsysis used in preliminary design. The motion of the typical section is represented by two degrees of freedom: pitch angle (θ) and vertical translation (ξ) – see Fig. 6 for conventions. The aeroelastic dynamics of this model are governed by (in dimensionless form):

$$M\ddot{\boldsymbol{\eta}} + K\boldsymbol{\eta} = \frac{V_\mu^2}{\pi} Q_a(\boldsymbol{\eta}_a), \tag{12a}$$

$$\dot{\boldsymbol{\eta}}_a = \mathcal{A}(M_\infty, \boldsymbol{\eta}_a, \boldsymbol{\eta}), \tag{12b}$$

[†]As mentioned above, this method is based on the algorithm CLoVER [46]. An open source implementation of CLoVER is available at `https://github.com/anmarques/CLoVER`

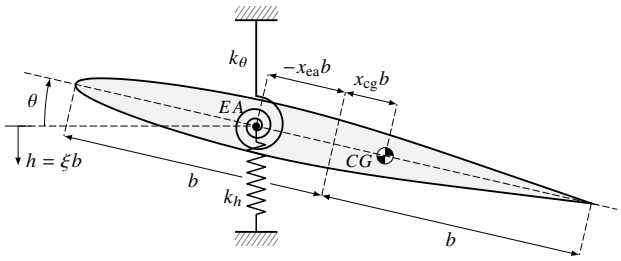

Fig. 6 Typical section model.

where

$$\boldsymbol{\eta} = \begin{Bmatrix} \theta \\ \xi \end{Bmatrix}, \quad M = \begin{bmatrix} 1 & \boldsymbol{x}_\theta \\ \boldsymbol{x}_\theta & r_\theta^2 \end{bmatrix}, \quad K = \begin{bmatrix} (\omega_h/\omega_\theta)^2 & 0 \\ 0 & r_\theta^2 \end{bmatrix}, \quad Q_a = \begin{Bmatrix} -c_\ell \\ 2c_m \end{Bmatrix}. \tag{13}$$

In the equation above, $x_\theta = x_{cg} - x_{ea}$, where x_{cg} denotes the position of the center of gravity and x_{ea} the position of the elastic axis, both measured from the mid-chord and non-dimensionalized with respect to the semi-chord b. Furthermore, r_θ is the radius of gyration per unit span about the elastic axis, ω_h and ω_θ are the uncoupled natural angular frequencies of vibration of the heave and pitch modes, respectively. c_ℓ denotes lift coefficient, and c_m denotes momentum coefficient with respect to the elastic axis. Finally,

$$V_\mu = \frac{V_\infty b}{\omega_\theta \sqrt{\mu}}, \quad \mu = \frac{m_a}{\pi \rho_\infty b^2},$$

where ρ_∞ and V_∞ are the density and speed at freestream, respectively, and m_a is the mass of the airfoil per unit span.

The case A problem of Isogai [50] is defined by the following set of parameters:

$$\mu = 60, \quad r_\theta^2 = 3.48, \quad \omega_h = 100\,\text{rad/s}, \quad \omega_\theta = 100\,\text{rad/s}, \quad x_{cg} = -0.2, \quad x_{ea} = -2.$$

In this investigation we assume the airflow is in the high Reynolds number regime, such that it is reasonable to neglect viscous effects. We investigate the aeroelastic flutter boundary as a function of two aerodynamic parameters: Mach number (M_∞) and aeroelastic speed index (V_μ). We restrict the parameter space to $(M_\infty, V_\mu) \in [0.6, 0.9] \times [0.4, 2.0]$, which is known to include the transonic dip phenomenon for this particular problem.

B. Aeroelastic models

We use four aeroelastic models to perform the aeroelastic flutter analysis of the Isogai case A problem. Three of these models are based on integrating (12) in time using the open source code SU2 [52], employing the Euler equations as the formulation of the airflow dynamics. Evaluations of these models start by computing a steady aerodynamic solution at angle-of-attack of 1 degree, and using this solution as initial condition for the unsteady aeroelastic simulation. These models are distinct in their computational meshes and solution time, as listed below. We define the solution time in terms of the period of the uncoupled vibration of the pitch mode: $T_\theta = 2\pi/\omega_\theta$.

For aeroelastic models based on SU2, we estimate the aeroelastic damping coefficient by fitting the response of the system to

$$\boldsymbol{\eta}(t) = \boldsymbol{\eta}_0 + \exp(d_1 t)\Big(\boldsymbol{\eta}_{11}\sin(\omega_1 t) + \boldsymbol{\eta}_{12}\cos(\omega_1 t)\Big) + \exp(d_2 t)\Big(\boldsymbol{\eta}_{21}\sin(\omega_2 t) + \boldsymbol{\eta}_{22}\cos(\omega_2 t)\Big),$$

where $\boldsymbol{\eta}_{jk}$ corresponds to the k-th component of the j-th aeroelastic mode. Associated to each mode j there is a corresponding damping d_j, angular frequency ω_j, amplitude $(\boldsymbol{\eta}_{j1}^2 + \boldsymbol{\eta}_{j2}^2)^{1/2}$, and phase angle $\tan^{-1}(\boldsymbol{\eta}_{j2}/\boldsymbol{\eta}_{j1})$.

The fourth model is based on solving (12) in Laplace domain using the p-k method [13]. The aerodynamic forces are estimated using the doublet lattice method [53].

The list below summarizes the computational models used in the present multifidelity analysis[‡]:

- High-fidelity model (HFM): time integration using SU2, Euler equations, fine mesh (8606 points). Solution time: $10T_\theta$. Computational cost: $\approx 27{,}000$ CPU-s.

[‡]Computational cost measured on an Intel® Core™ i7-2600 CPU (3.4 GHz). Simulations are carried out on a single core.

- Low-fidelity model 1 (LFM1): time integration using SU2, Euler equations, fine mesh (8606 points), Solution time: $3T_\theta$. Computational cost: $\approx 9,000$ CPU-s.
- Low-fidelity model 2 (LFM2): time integration using SU2, Euler equations, coarse mesh (4572 points). Solution time: $3T_\theta$. Computational cost: $\approx 2,700$ CPU-s.
- Low-fidelity model 3 (LFM3): Laplace domain using p-k method, doublet lattice method (30 panels). Computational cost: ≈ 10 CPU-s.

C. Aeroelastic flutter boundary

We initialize the multifidelity method by evaluating all four aeroelastic models at ten random configurations. These evaluations are used to estimate the hyperparameters and provide initial training data to the surrogate model. In this example we use the same form of Gaussian process prior for the high-fidelity function and the discrepancies. Namely, we set the mean function to zero, and choose a squared exponential covariance kernel [48]. The top left frame of Fig. 7 shows the initial setup.

As discussed in Sect. III, we solve the optimization problem (9) to select new evaluations at every iteration of the multifidelity method. Here we solve the optimization problem by performing a search on a uniform $4 \times 30 \times 30$ grid in the space $(\ell, M_\infty, V_\mu) \in \{0, 1, 2, 3\} \times [0.6, 0.9] \times [0.4, 2]$. Figure 7 shows the local entropy $H(W_{\boldsymbol{x}})$ at a few snapshots of the iteration procedure. This figure also shows the sets of configurations used to evaluate models HFM, LFM1, and LFM2. For the sake of clarity, we omit evaluations of LFM3 because they would clutter the plots.

For the purposes of comparison, we compute a reference flutter boundary. This reference is computed using our multifidelity method with a high budget (approximately 42 HFM evaluations). We then demonstrate our multifidelity method by limiting the total budget to approximately 32 HFM. This number was chosen because it represents the cost of the initial setup (approximately 11 HFM evaluations) plus using a bisection method to estimate 3 points on the aeroelastic flutter boundary, considering a budget of 7 HFM evaluations per point.[§] Figure 8 shows the evolution of the estimate of the flutter boundary using the multifidelity method. We observe that the method produces accurate estimates, with a maximum error smaller than 0.02 in flutter speed index.

The exception is the region at the top right corner of the domain (high Mach number and high speed index). SU2 predicts that the flutter boundary wraps around itself, allowing the aeroelastic system to become stable when the speed index is increased at high Mach number (≈ 0.9). This phenomenon has been reported in the literature [1]. This wrapping of the aeroelastic flutter boundary leads to relatively large gradients in the aeroelastic damping coefficient at high Mach number. The multifidelity method requires more evaluations than the set budget to estimate this behavior adequately.

Our proposed method combines both adaptive sampling and the use of multiple aeroelastic models. To assess directly the benefits of using multiple aeroelastic models, we compare the performance of our method using all four models to its performance using only a single aeroelastic model (the HFM). Figure 9 shows the aeroelastic flutter boundaries estimated with a single model, and Fig. 10 compares the evolution of the contour entropy per computational cost when considering a single and multiple models. We observe that the estimates produced with a single aeroelastic model are similar to the ones produced using multiple aeroelastic models. This result indicates that, for this particular problem, using an active learning framework to select new evaluations has a greater impact on the accuracy of predictions of the aeroelastic flutter boundary than considering multiple aeroelastic models. However, using multiple models results in a lower value of contour entropy, which indicates that the method has more confidence in its prediction.

We explain these results in light of the choice of Gaussian process prior used for this analysis. The prior model selected here contained no specific information about the location of the aeroelastic flutter boundary. Hence, the multifidelty method has to explore the entire space of possible aeroelastic configurations to gain confidence in the predictions it makes. As we can observe from Fig. 7, if multiple aeroelastic models are available, the method uses the low-fidelity models to explore the space, and evaluates the high-fidelity model close to the aeroelastic flutter boundary to increase the accuracy in its vicinity. This behavior explains why the method is more confident in the estimates made with multiple aeroelastic models: the additional models allow the method to explore more of the space than it can afford using a single aeroelastic model. These results indicate future research on adequate prior models specific for aeroelastic applications is needed to take full advantage of multiple aeroelastic models.

[§]For the range of V_μ considered here, a bisection method with 7 HFM evaluations can predict the speed index at flutter with accuracy of 0.0125, for each Mach number.

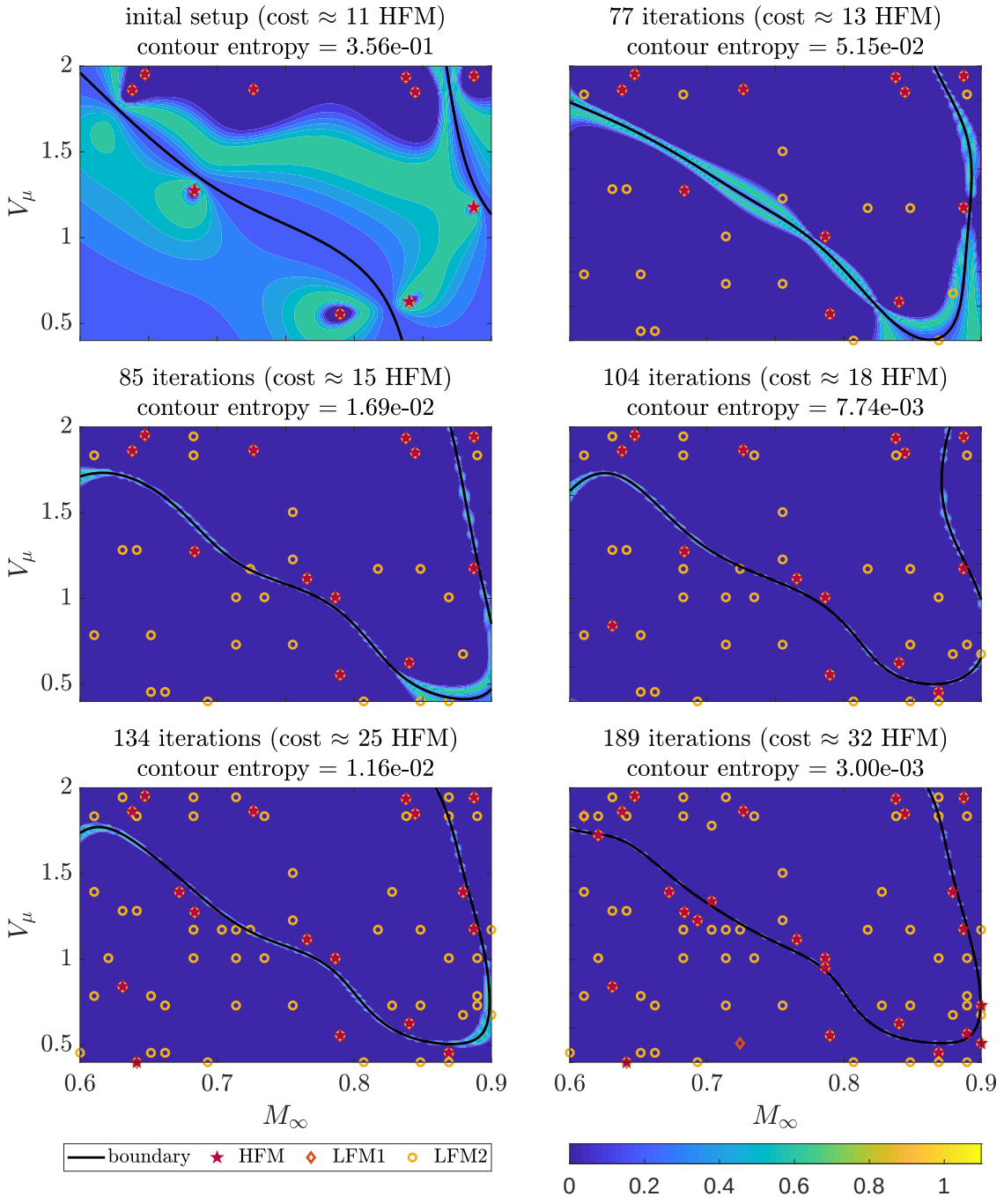

Fig. 7 Locating the flutter boundary of the Isogai case A problem. Each plot shows the estimates of the multifidelity method for different iterations. The solid black line is the aeroelastic flutter boundary estimated by the multifidelity method. The contours show the local value of the entropy $H(W_x)$. The symbols are evaluations made with the different aeroelastic models.

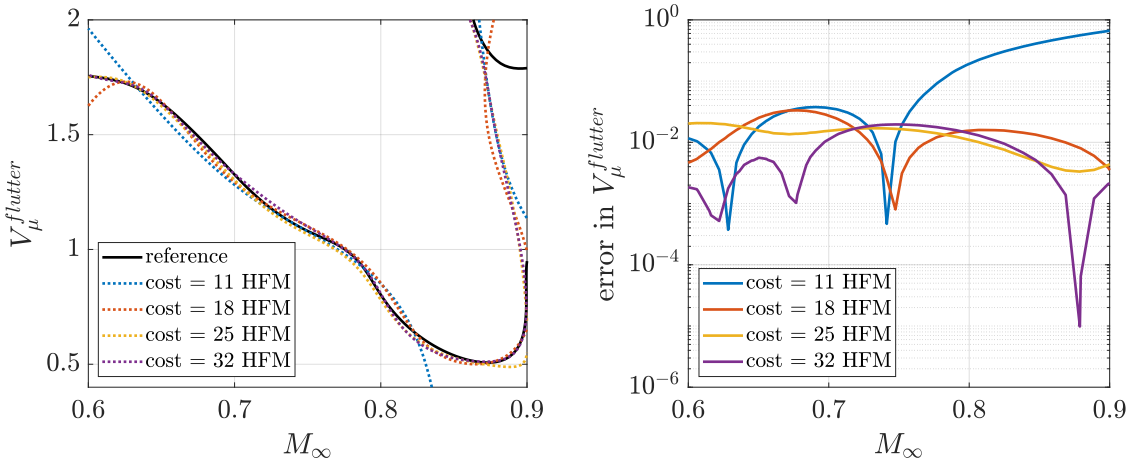

Fig. 8 Aeroelastic flutter boundaries estimated by the multifidelity method at different levels of cost. $V_\mu^{flutter}$ is the speed index at the aeroelastic flutter boundary. Left: position of flutter boundaries. Right: error in the $V_\mu^{flutter}$ with respect to the reference computed with a cost equivalent to 42 HFM evaluations. The error only considers the aeroelastic flutter boundary corresponding the the smallest flutter speed index for each Mach number.

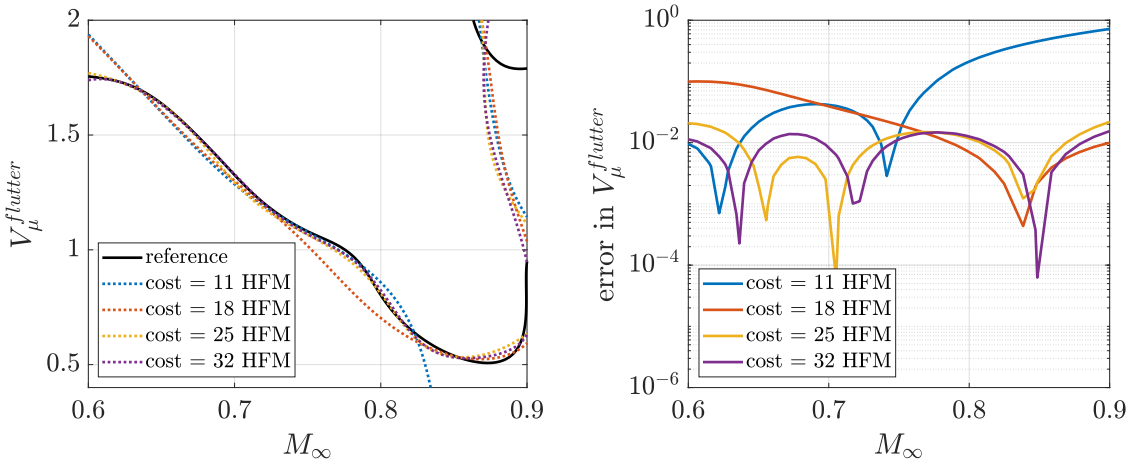

Fig. 9 Aeroelastic flutter boundaries estimated by the method presented here evaluated with a single aeroelastic model (HFM), at different levels of cost. $V_\mu^{flutter}$ is the speed index at the aeroelastic flutter boundary. Left: position of flutter boundaries. Right: error in the $V_\mu^{flutter}$ with respect to the reference computed with a cost equivalent to 42 HFM evaluations. The error only considers the aeroelastic flutter boundary corresponding the the smallest flutter speed index for each Mach number.

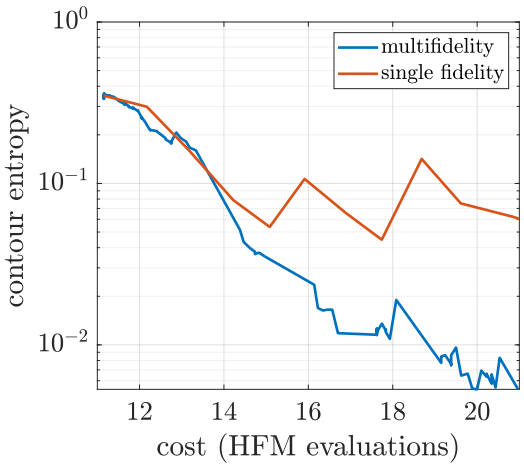

Fig. 10 Evolution of contour entropy per computational cost. Comparison between results obtained with a single aeroelastic model (single fidelity) and multiple models (multifidelity).

V. Conclusion

We presented a mutlifidelity method that locates aeroelastic flutter boundaries by combining information from low- and high-fidelity aeroelastic models. We demonstrated through an example of the typical section model that this method can result in significant computational savings with respect to a naive exploration of the space of aeroelastic configurations (e.g., bisection method). However, further investigation is still needed to take full advantage of the multifidelity framework for aeroelastic applications.

There are few possibilities for extending the work shown here. First, estimating the aeroelastic damping coefficient from time histories is challenging when damping is very small in magnitude (close to the flutter boundary) or very large (unstable regions). Quantifying the uncertainty in these estimates may make the multifidelity method more robust. Second, here we assume that the cost of evaluating the aeroelastic models is known. However, in practice simulations in unstable regions may terminate early because they result in large oscillations, and estimating the computational cost a priori is difficult. An alternative is using data to create a surrogate model for the computational cost as well. This approach may lead to different strategies for acquiring data, since the utility function used to select the next model to evaluate depends both on expected information gain (i.e., entropy reduction) and on model cost. Finally, investigating prior GP models tailored to aeroelastic applications may allow the multifidelity method to use information from multiple aeroelastic models more efficiently.

Acknowledgments

This work was supported in part by the U.S. Air Force Center of Excellence on Multi-Fidelity Modeling of Rocket Combustor Dynamics, Award FA9550-17-1-0195, and by the AFOSR MURI on Managing Multiple Information Sources of Multi-Physics Systems, Awards FA9550-15-1-0038 and FA9550-18-1-0023.

References

[1] Alonso, J. J., and Jameson, A., "Fully-Implicit Time-Marching Aeroelastic Solutions," *32nd Aerospace Sciences Meeting and Exhibit*, AIAA, Reno, NV, 1994. doi:10.2514/6.1994-56.

[2] Liu, F., Cai, J., Y. Z., Tsai, H. M., and Wong, A. S. F., "Calculation of Wing Flutter by a Coupled Fluid-Structure Method," *Journal of Aircraft*, Vol. 38, No. 2, 2001, pp. 334–342. doi:10.2514/2.2766.

[3] Farhat, C., "CFD on moving grids: from theory to realistic flutter, maneuvering, and multidisciplinary optimization," *International Journal of Computational Fluid Dynamics*, Vol. 19, No. 8, 2005, pp. 595–603. doi:10.1080/10618560500510579.

[4] Datta, A. D., Sitaraman, J., Chopra, I., and Baeder, J. D., "Consistent rational-function approximation for unsteady aerodynamics," *Journal of Aircraft*, Vol. 28, No. 9, 1991, pp. 545–552. doi:10.2514/3.46062.

[5] Bazilevs, Y., Calo, V. M., Hughes, T. J. R., and Zhang, Y., "Isogeometric fluid-structure interaction: theory, algorithms, and computations," *Computational Mechanics*, Vol. 43, No. 1, 2008, pp. 3–37. doi:10.1007/s00466-008-0315-x.

[6] Hou, G., Wang, J., and Layton, A., "Numerical Methods for Fluid-Structure Interaction — A Review," *Communications in Computational Physics*, Vol. 12, No. 2, 2012, pp. 337—-377. doi:10.4208/cicp.291210.290411s.

[7] Smith, M. J., Lim, J. W., van der Wall, B. G., Baeder, J. D., Biedron, R. T., Boyd, D. D., Jayaraman, B., Jung, S. N., and Min, B.-Y., "The HART II international workshop: an assessment of the state of the art in CFD/CSD prediction," *CEAS Aeronautical Journal*, Vol. 4, No. 4, 2013, pp. 345–372. doi:10.1007/s13272-013-0078-8.

[8] Heeg, J., "Overview and Lessons Learned from the Aeroelastic Prediction Workshop," *54th AIAA/ASME/ASCE/AHS/ASC Structures, Structural Dynamics, and Materials Conference*, AIAA, Boston, MA, 2013. doi:10.2514/6.2013-1798.

[9] Heeg, J., Chwalowski, P., Raveh, D. E., Jirasek, A., and Dalenbring, M., "Overview and Data Comparisons from the 2nd Aeroelastic Prediction Workshop," *34th AIAA Applied Aerodynamics Conference (AIAA Aviation Forum)*, AIAA, Washington, DC, 2016. doi:10.2514/6.2016-3121.

[10] Farhat, C., *CFD-Based Nonlinear Computational Aeroelasticity*, American Cancer Society, 2017, pp. 1–21. doi:10.1002/9781119176817.ecm2063.

[11] Miller, B. A., and McNamara, J. J., "Efficient Fluid-Thermal-Structural Time Marching with Computational Fluid Dynamics," *Journal of Aircraft*, Vol. 56, No. 9, 2018, pp. 3610–3621. doi:10.2514/1.J056572.

[12] Bisplinghoff, R. L., Ashley, H., and Halfman, R. L., *Aeroelasticity*, Dover Publications, Mineola, New York, 1996.

[13] Hassig, H. J., "An Approximate True Damping Solution of the Flutter Equation by Determinant Iteration," *Journal of Aircraft*, Vol. 8, No. 11, 1971, pp. 885–889. doi:10.2514/3.44311.

[14] Roddenj, W. P., Giesing, J. P., and Kálmán, T. P., "Refinement of the nonplanar aspects of the subsonic doublet-lattice lifting surface method," *Journal of Aircraft*, Vol. 9, No. 1, 1972, pp. 69–73. doi:10.2514/3.44322.

[15] Giesing, J. P., Kálmán, T. P., and Roddenj, W. P., "Subsonic Steady and Oscillatory Aerodynamics for Multiple Interfering Wings and Bodies," *Journal of Aircraft*, Vol. 9, No. 10, 1972, pp. 693–702. doi:10.2514/3.59066.

[16] Drela, M., "Integrated simulation model for preliminary aerodynamic, structural, and control-law design of aircraft," *40th Structures, Structural Dynamics, and Materials Conference and Exhibit, Structures, Structural Dynamics, and Materials*, AIAA, St. Louis, MO, 1999. doi:10.2514/6.1999-1394.

[17] Roger, K. L., "Airplane Math Modeling Methods for Active Control Design," Tech. Rep. AGARD–CP–228, Aug 1977.

[18] Abel, I., "An Analytical Technique for Predicting the Characteristics of a Flexible Wing Equipped with an Active Flutter-Suppression System and Comparison with Wind-Tunnel Data," Tech. Rep. NASA TP–1367, Feb 1979.

[19] Dunn, H. J., "An Analytical Technique for Approximating Unsteady Aerodynamic in the Time Domain," Tech. Rep. NASA TP–1738, Nov 1980.

[20] Eversman, W., and Tewari, A., "Consistent rational-function approximation for unsteady aerodynamics," *Journal of Aircraft*, Vol. 28, No. 9, 1991, pp. 545–552. doi:10.2514/3.46062.

[21] Fidkowski, K., Kroo, I., Willcox, K., and Engelson, F., "Stochastic Gust Analysis Techniques for Aircraft Conceptual Design," *12th AIAA/ISSMO Multidisciplinary Analysis and Optimization Conference*, AIAA, Victoria, British Columbia, Canada, 2008. doi:10.2514/6.2008-5848.

[22] Marques, A. N., and Azevedo, J. L. F., "Numerical Calculation of Impulsive and Indicial Aerodynamic Responses Using Computational Aerodynamics Techniques," *Journal of Aircraft*, Vol. 45, No. 4, 2008, pp. 1112–1135. doi:10.2514/1.32151.

[23] Marques, A. N., and Azevedo, J. L. F., "A z Transform Discrete-Time State Space Formulation for Aeroelastic Stability Analysis," *Journal of Aircraft*, Vol. 45, No. 5, 2008, pp. 1564–1578. doi:10.2514/1.32561.

[24] Chen, P. C., Zhang, Z., and Eli, L., "Design-Oriented Computational Fluid Dynamics-Based Unsteady Aerodynamics for Flight-Vehicle Aeroelastic Shape Optimization," *Journal of Aircraft*, Vol. 53, No. 12, 2015, pp. 3603–3619. doi:10.2514/1.J054024.

[25] Opgenoord, M. M. J., Drela, M., and Willcox, K. E., "Physics-Based Low-Order Model for Transonic Flutter Prediction," *AIAA Journal*, Vol. 56, No. 4, 2018, pp. 1519–1531. doi:10.2514/1.J056710.

[26] Benner, P., Gugercin, S., and Willcox, K., "A Survey of Projection-Based Model Reduction Methods for Parametric Dynamical Systems," *SIAM Review*, Vol. 57, No. 4, 2015, pp. 483–531. doi:10.1137/130932715.

[27] Sirovich, L., "Turbulence and the Dynamics of Coherent Structures. Part 1: Coherent Structures," *Quarterly of Applied Mathematics*, Vol. 45, No. 3, 1987, pp. 561–571. doi:10.1090/qam/910462.

[28] Berkooz, G., Holmes, P., and Lumley, J. L., "The Proper Orthogonal Decomposition in the Analysis of Turbulent Flows," *Annual Review of Fluid Mechanics*, Vol. 25, 1993, pp. 539–575. doi:10.1146/annurev.fluid.25.1.539.

[29] Dowell, E. H., and Hall, K. C., "Modeling of Fluid-Structure Interaction," *Annual Review of Fluid Mechanics*, Vol. 33, No. 1, 2001, pp. 445–490. doi:10.1146/annurev.fluid.33.1.445.

[30] Thomas, J. P., Dowell, E. H., and Hall, K. C., "Modeling Viscous Transonic Limit Cycle Oscillation Behavior using a Harmonic Balance Approach," *Journal of Aircraft*, Vol. 41, No. 6, 2004, pp. 1266–1274. doi:10.2514/1.9839.

[31] Silva, W. A., "Application of Nonlinear Systems Theory to Transonic Unsteady Aerodynamic Responses," *Journal of Aircraft*, Vol. 30, No. 5, 1993, pp. 660–668. doi:10.2514/3.46395.

[32] Opgenoord, M. M. J., "Transonic Flutter Prediction and Aeroelastic Tailoring for Next-Generation Transport Aircraft," Ph.D. thesis, Department of Aeronautics & Astronautics, Massachusetts Institute of Technology, 9 2018.

[33] Settles, B., "Active learning," *Synthesis Lectures on Artificial Intelligence and Machine Learning*, Vol. 6, No. 1, 2012, pp. 1–114.

[34] Cortes, C., and Vapnik, V., "Support-vector networks," *Machine Learning*, Vol. 20, No. 3, 1995, pp. 273–297. doi:10.1007/BF00994018.

[35] Basudhar, A., Missoum, S., and Sanchez, A. H., "Limit state function identification using Support Vector Machines for discontinuous responses and disjoint failure domains," *Probabilistic Engineering Mechanics*, Vol. 23, No. 1, 2008, pp. 1–11. doi:10.1016/j.probengmech.2007.08.004.

[36] Basudhar, A., and Missoum, S., "An improved adaptive sampling scheme for the construction of explicit boundaries," *Structural and Multidisciplinary Optimization*, Vol. 42, No. 4, 2010, pp. 517–529. doi:10.1007/s00158-010-0511-0.

[37] Lecerf, M., Allaire, D., and Willcox, K., "Methodology for Dynamic Data-Driven Online Flight Capability Estimation," *AIAA Journal*, Vol. 53, No. 10, 2015, pp. 3073–3087. doi:10.2514/1.J053893.

[38] Missoum, S., Dribusch, C., and Beran, P., "Reliability-Based Design Optimization of Nonlinear Aeroelasticity Problems," *Journal of Aircraft*, Vol. 47, No. 3, 2010, pp. 992–998. doi:10.2514/1.46665.

[39] Dribusch, C., Missoum, S., and Beran, P., "A multifidelity approach for the construction of explicit decision boundaries: application to aeroelasticity," *Structural and Multidisciplinary Optimization*, Vol. 42, No. 5, 2010, pp. 693–705. doi:10.1007/s00158-010-0516-8.

[40] Bichon, B. J., Eldred, M. S., Swiler, L. P., Mahadevan, S., and McFarland, J. M., "Efficient Global Reliability Analysis for Nonlinear Implicit Performance Functions," *AIAA Journal*, Vol. 46, No. 10, 2008, pp. 2459–2468. doi:10.2514/1.34321.

[41] Ranjan, P., Bingham, D., and Michailidis, G., "Sequential Experiment Design for Contour Estimation From Complex Computer Codes," *Technometrics*, Vol. 50, No. 4, 2008, pp. 527–541. doi:10.1198/004017008000000541.

[42] Picheny, V., Ginsbourger, D., Roustant, O., Haftka, R. T., and Kim, N.-H., "Adaptive Designs of Experiments for Accurate Approximation of a Target Region," *Journal of Mechanical Design*, Vol. 132, No. 7, 2010. doi:10.1115/1.4001873.

[43] Bect, J., Ginsbourger, D., Li, L., Picheny, V., and Vazquez, E., "Sequential design of computer experiments for the estimation of a probability of failure," *Statistics and Computing*, Vol. 22, No. 3, 2012, pp. 773–793. doi:10.1007/s11222-011-9241-4.

[44] Chevalier, C., Bect, J., Ginsbourger, D., Vazquez, E., Picheny, V., and Richet, Y., "Fast Parallel Kriging-Based Stepwise Uncertainty Reduction With Application to the Identification of an Excursion Set," *Technometrics*, Vol. 56, No. 4, 2014, pp. 455–465. doi:10.1080/00401706.2013.860918.

[45] Wang, H., Lin, G., and Li, J., "Gaussian process surrogates for failure detection: A Bayesian experimental design approach," *Journal of Computational Physics*, Vol. 313, 2016, pp. 247–259. doi:10.1016/j.jcp.2016.02.053.

[46] Marques, A., Lam, R., and Willcox, K., "Contour location via entropy reduction leveraging multiple information sources," *Advances in Neural Information Processing Systems 31*, edited by S. Bengio, H. Wallach, H. Larochelle, K. Grauman, N. Cesa-Bianchi, and R. Garnett, Curran Associates, Inc., 2018, pp. 5222–5232.

[47] Poloczek, M., Wang, J., and Frazier, P., "Multi-Information Source Optimization," *Advances in Neural Information Processing Systems 30*, Curran Associates, Inc., 2017, pp. 4291–4301.

[48] Rasmussen, C. E., and Williams, C. K. I., *Gaussian Processes for Machine Learning (Adaptive Computation and Machine Learning)*, The MIT Press, 2005.

[49] Cover, T. M., and Thomas, J. A., *Elements of Information Theory (Wiley Series in Telecommunications and Signal Processing)*, Wiley-Interscience, 2006.

[50] Isogai, K., "On the Transonic-dip Mechanism of Flutter of a Sweptback Wing," *AIAA Journal*, Vol. 17, No. 7, 1979, pp. 793–795. doi:10.2514/3.61226.

[51] Dowell, E. H., *A Modern Course in Aeroelasticity*, Kluwer Academic Publishers, Dordrecht, The Netherlands, 2014. doi:10.1007/1-4020-2106-2.

[52] Economon, T. D., Palacios, F., Copeland, S. R., Lukaczyk, T. W., and Alonso, J. J., "SU2: An Open-Source Suite for Multiphysics Simulation and Design," *AIAA Journal*, Vol. 54, No. 3, 2016, pp. 828–846. doi:10.2514/1.J053813.

[53] Albano, E., and Hodden, W. P., "A Doublet-Lattice Method for Calculating Lift Distributions on Oscillating Surfaces in Subsonic Flows," *AIAA Journal*, Vol. 7, No. 2, 1969, pp. 279–285. doi:10.2514/3.5086.